Journal of Biomolecular NMR, 9 (1997) 287–298
ESCOM

J-Bio NMR 419

Rotational diffusion anisotropy of proteins from simultaneous analysis of ^{15}N and $^{13}C^{\alpha}$ nuclear spin relaxation

Larry K. Lee[a], Mark Rance[b], Walter J. Chazin[c] and Arthur G. Palmer III[a,*]

[a]*Department of Biochemistry and Molecular Biophysics, Columbia University, 630 West 168th Street, New York, NY 10032, U.S.A.*
[b]*Department of Molecular Genetics, Biochemistry, and Molecular Biology, University of Cincinnati, Cincinnati, OH 45267, U.S.A.*
[c]*Department of Molecular Biology, The Scripps Research Institute, 10666 North Torrey Pines Road, La Jolla, CA 92037, U.S.A.*

Received 23 September 1996
Accepted 29 November 1996

Keywords: Proteins; Nuclear spin relaxation; Rotational diffusion tensor anisotropy

Summary

Current methods of determining the rotational diffusion tensors of proteins in solution by NMR spectroscopy exclusively utilize relaxation rate constants for backbone amide ^{15}N spins. However, the distributions of orientations of N-H bond vectors are not isotropic in many proteins, and correlations between bond vector orientations reduce the accuracy and precision of rotational diffusion tensors extracted from ^{15}N spin relaxation data. The inclusion of both $^{13}C^{\alpha}$ and ^{15}N spin relaxation rate constants increases the robustness of the diffusion tensor analysis because the orientations of the C^{α}-H^{α} bond vectors differ from the orientations of the N-H bond vectors. Theoretical and experimental results for calbindin D_{9k}, granulocyte colony stimulating factor, and ubiquitin, three proteins with different distributions of N-H and C^{α}-H^{α} bond vectors, are used to illustrate the advantages of the simultaneous utilization of $^{13}C^{\alpha}$ and ^{15}N relaxation data.

Introduction

NMR spectroscopy is sensitive to motional processes in molecules through the phenomenon of nuclear spin relaxation. Intramolecular motions in proteins are amenable to investigation by use of ^{15}N, ^{13}C, and ^{2}H spin relaxation (Palmer et al., 1996). Typically, relaxation data are analyzed by modeling the power spectral density function with the model-free (Lipari and Szabo, 1982a,b) or spectral density mapping formalisms (Peng and Wagner, 1992; Farrow et al., 1995; Ishima and Nagayama, 1995). The majority of these studies concern approximately spherical globular proteins and isotropic overall rotational diffusion has been assumed. Rotational diffusion anisotropy has a profound effect on the physics of spin relaxation and on the interpretation of experimental studies of intramolecular dynamics because the power spectral density function depends on the relative orientations of the principal axis systems of the operant relaxation mechanisms and the diffusion tensor (Woessner, 1962). Consequently, an experimental knowledge of the rotational diffusion tensor is essential for a detailed analysis of intramolecular motions in nonspherical proteins. In addition, experimental investigations of rotational diffusion anisotropy can provide information on the conformations of multidomain proteins and can monitor alterations in the hydrodynamic properties of proteins following ligation or allosteric conformational changes (Brüschweiler et al., 1995).

Rotational diffusion anisotropies for several proteins have been determined from ^{15}N relaxation measurements (Brüschweiler et al., 1995; Tjandra et al., 1995; Zheng et al., 1995; Mackay et al., 1996). Two methods of determining the diffusion tensor have emerged: direct fitting of the R_2/R_1 ratios for a set of nuclear spins, in which R_1 is the spin-lattice relaxation rate constant and R_2 is the spin-spin relaxation rate constant (Tjandra et al., 1995; Zheng et al., 1995); and analysis of local diffusion coefficients that are derived in turn from relaxation rate constants (Brüschweiler et al., 1995). However, due to the constraints imposed by hydrogen bonding in secondary structures, the orientations of the N-H bond vectors are not distributed isotropically in many proteins. Correla-

*To whom correspondence should be addressed.

tions between the orientations of the N-H bond vectors compromise the accuracy and precision of the diffusion tensor derived from NMR relaxation measurements.

The present paper demonstrates that simultaneous analysis of $^{13}C^{\alpha}$ and ^{15}N relaxation rate constants improves the reliability of the diffusion tensor determination, both because the distribution of the orientations of bond vectors is more ideal and because the quantity of data is increased. Representation of the local diffusion constants in quadratic form (Brüschweiler et al., 1995) is convenient for simultaneous analysis of relaxation data acquired for multiple nuclear species or magnetic field strengths. Additional results concerning this formalism are provided, and simple relationships diagnostic of the distribution of bond vector orientations are derived. Relaxation data for calbindin D_{9k} (Kördel et al., 1992), granulocyte colony stimulating factor (G-CSF) (Zink et al., 1994), and ubiquitin (Tjandra et al., 1995), three proteins with distinct distributions of bond vector orientations, are analyzed to illustrate the approach empirically and theoretically.

Theory

Rate constants for spin-lattice relaxation (R_1), spin-spin relaxation (R_2), and dipolar cross-relaxation (σ) can be determined for backbone $^{13}C^{\alpha}$ or ^{15}N spins in proteins by using standard inverse-detected multidimensional NMR experiments (Skelton et al., 1993; Farrow et al., 1994). The relaxation rate constants for the *i*th $^{13}C^{\alpha}$ or ^{15}N spin are given by (Abragam, 1961)

$$\begin{aligned} R_{1i} &= q_{DD}\{J_i(\omega_X-\omega_H) + 3J_i(\omega_X) + 6J_i(\omega_X+\omega_H)\} \\ &\quad + q_{CSA}J_i(\omega_X) \\ R_{2i} &= (1/2)q_{DD}\{4J_i(0) + J_i(\omega_X-\omega_H) + 3J_i(\omega_X) \\ &\quad + 6J_i(\omega_H) + 6J_i(\omega_X+\omega_H)\} \\ &\quad + (1/6)q_{CSA}\{4J_i(0) + 3J_i(\omega_X)\} \\ \sigma_i &= q_{DD}\{6J_i(\omega_X+\omega_H) - J_i(\omega_X-\omega_H)\} \\ &= (\gamma_X/\gamma_H)(NOE-1)R_1 \end{aligned} \tag{1}$$

where $q_{DD}=(1/10)(\mu_0/4\pi)^2\hbar^2\gamma_X^2\gamma_H^2r_{XH}^{-6}$; $q_{CSA}=(2/15)\omega_X^2\Delta\sigma^2$; μ_0 is the permeability of free space; $\hbar$ is Planck's constant divided by 2π; ω_X and ω_H are the Larmor frequencies of the X ($X = {}^{13}C^{\alpha}$ or ^{15}N) and ^1H spins, respectively; γ_X and γ_H are the gyromagnetic ratios of the X and ^1H spins, respectively; r_{XH} is the internuclear N-H or C^{α}-H^{α} distance; $\Delta\sigma$ is the chemical shift anisotropy of the X spin; and NOE is the $\{^1H\}$-X steady-state nuclear Overhauser effect. The principal axes of the chemical shift tensors for ^{15}N and $^{13}C^{\alpha}$ spins are oriented nearly collinearly with the N-H and C^{α}-H^{α} bond vectors, respectively. The spectral density function, $J_i(\omega)$, can be expressed as the cosine transform of the correlation function of the normalized X-H bond vector (Abragam, 1961):

$$J_i(\omega) = \int_0^{\infty} \langle P_2[\mu_i(0)\cdot\mu_i(\tau)]\rangle \cos(\omega\tau)\, d\tau \tag{2}$$

where $P_2(x) = (3x^2-1)/2$, $\mu_i(t)$ is a unit vector along the X-H bond vector at time t, and $\langle\cdots\rangle$ indicates an ensemble average.

For bond vectors subject only to low-amplitude, rapid intramolecular motions, the R_{2i}/R_{1i} ratio is approximately independent of intramolecular dynamics and is given by (Kay et al., 1989; Tjandra et al., 1995; Zheng et al., 1995)

$$\begin{aligned} R_{2i}/R_{1i} = &\{4J_i(0) + J_i(\omega_X-\omega_H) + 3J_i(\omega_X) + 6J_i(\omega_H) \\ &+ 6J_i(\omega_X+\omega_H) + (q_{CSA}/3q_{DD})[4J_i(0) + 3J_i(\omega_X)]\}/ \\ &\{2J_i(\omega_X-\omega_H) + 6J_i(\omega_X) + 12J_i(\omega_X+\omega_H) \\ &+ 2(q_{CSA}/q_{DD})J_i(\omega_X)\} \end{aligned} \tag{3}$$

where $J_i(\omega)$ is the spectral density function for overall rotational diffusion. For an asymmetric top with an anisotropic diffusion tensor (Woessner, 1962),

$$J_i(\omega) = \sum_{j=1}^{5} A_{ji}\frac{\tau_j}{1+\omega^2\tau_j^2} \tag{4}$$

$$\begin{aligned} \tau_1 &= (4D_{xx} + D_{yy} + D_{zz})^{-1} \\ \tau_2 &= (D_{xx} + 4D_{yy} + D_{zz})^{-1} \\ \tau_3 &= (D_{xx} + D_{yy} + 4D_{zz})^{-1} \\ \tau_4 &= \{6D_{iso} + 6(D_{iso}^2 - L^2)^{1/2}\}^{-1} \\ \tau_5 &= \{6D_{iso} - 6(D_{iso}^2 - L^2)^{1/2}\}^{-1} \end{aligned} \tag{5}$$

$$\begin{aligned} A_{1i} &= 3y_i^2z_i^2 \\ A_{2i} &= 3x_i^2z_i^2 \\ A_{3i} &= 3x_i^2y_i^2 \\ A_{4i} &= (1/4)\{3(x_i^4+y_i^4+z_i^4) - 1\} \\ &\quad - (1/12)\{\delta_x(3x_i^4+6y_i^2z_i^2-1) + \delta_y(3y_i^4+6z_i^2x_i^2-1) \\ &\quad + \delta_z(3z_i^4+6x_i^2y_i^2-1)\} \\ A_{5i} &= (1/4)\{3(x_i^4+y_i^4+z_i^4) - 1\} \\ &\quad + (1/12)\{\delta_x(3x_i^4+6y_i^2z_i^2-1) + \delta_y(3y_i^4+6z_i^2x_i^2-1) \\ &\quad + \delta_z(3z_i^4+6x_i^2y_i^2-1)\} \end{aligned} \tag{6}$$

where D_{xx}, D_{yy}, and D_{zz} are the principal values of the diffusion tensor $\mathbf{D}$, $D_{iso} = \text{Trace}\{\mathbf{D}\}/3 = (D_{xx}+D_{yy}+D_{zz})/3$, $L^2 = (D_{xx}D_{yy}+D_{xx}D_{zz}+D_{yy}D_{zz})/3$, $\delta_k = (D_{kk}-D_{iso})/(D_{iso}^2-L^2)^{1/2}$ (for $k = x,y,z$), and $\mathbf{e}_i = (x_i,y_i,z_i)$ are the direction cosines defining the orientation of the *i*th X-H bond vector in the principal axis frame of the diffusion tensor. For a sym-

metric top with an axially symmetric diffusion tensor, $D_\perp = D_{xx} = D_{yy}$ and $D_\parallel = D_{zz}$ are the two unique diffusion coefficients, $D_{iso} = (D_\parallel + 2D_\perp)/3$, and (Woessner, 1962)

$$J_i(\omega) = \sum_{j=1}^{3} A_{ji} \frac{\tau_j}{1+\omega^2\tau_j^2} \tag{7}$$

where $\tau_1^{-1} = 6D_\perp$, $\tau_2^{-1} = 5D_\perp + D_\parallel$, $\tau_3^{-1} = 2D_\perp + 4D_\parallel$, $A_{1i} = (3\cos^2\theta_i - 1)^2/4$, $A_{2i} = 3\sin^2\theta_i\cos^2\theta_i$, $A_{3i} = (3/4)\sin^4\theta_i$, and θ_i is the angle between the X-H bond for the *i*th spin and the unique axis of the principal frame of the diffusion tensor. For a spherical top with an isotropic diffusion tensor, $D_{iso} = D_{xx} = D_{yy} = D_{zz}$ is the isotropic diffusion constant, and (Woessner, 1962)

$$J_i(\omega) = J(\omega) = \frac{\tau_c}{1+\omega^2\tau_c^2} \tag{8}$$

where $\tau_c = (6D_{iso})^{-1}$. As shown, $J_i(\omega)$ is independent of the orientation of the X-H bond vector.

An experimental data set consists of relaxation rate constants, R_{1i} and R_{2i}, and the direction cosines, $\mathbf{e}_i$, for i = 1 to N spins. The direction cosines are derived from the coordinates of the X-H bond vector in an arbitrary molecular reference frame (usually determined by the coordinate frame of a molecular model of the protein as determined by X-ray crystallography or NMR spectroscopy). The molecular frame does not normally coincide with the principal axis frame of the diffusion tensor (other than for the isotropic model), and a coordinate transformation between the two frames must be executed. For the axially symmetric model, the angles θ and ϕ define the orientation of the unique axis of the diffusion tensor frame relative to the arbitrary molecular frame. For the anisotropic model, the Euler angles, θ, ϕ, and ψ, define the orientation of the diffusion tensor frame relative to the arbitrary molecular frame. Equation 3 can be solved directly by nonlinear least-squares optimization to determine D_{iso} for the isotropic model; $D_\perp$, $D_\parallel$, θ, and ϕ for the axially symmetric model; and D_{xx}, D_{yy}, D_{zz}, θ, ϕ, and ψ for the anisotropic model (or appropriate combinations of these variables) (Tjandra et al., 1995; Zheng et al., 1995). A χ^2 variable is defined to statistically evaluate the goodness-of-fit of the diffusion models and an F-statistic is used to discriminate between isotropic, axially symmetric, and anisotropic models (vide infra).

Alternatively, a local diffusion constant, $D_i = (6\tau_{ci})^{-1}$, is defined for the *i*th spin for i = 1,...,N by fitting the isotropic diffusion model individually to each R_{2i}/R_{1i} ratio using Eqs. 3 and 8 or by fitting the Lipari–Szabo model-free spectral density function (Lipari and Szabo, 1982a,b) to the experimental R_{1i}, R_{2i}, and σ_i data (Brüschweiler et al., 1995). Local diffusion constants have been used to characterize qualitatively motional anisotropy in calmodulin (Barbato et al., 1992) and to approximate the degree of rotational anisotropy in proteins (Schurr et al., 1994). A quantitative treatment was provided by Brüschweiler et al. (1995), who stated that, for small anisotropies of the diffusion tensor **D**, the D_i have a quadratic form in an arbitrary reference frame:

$$D_i = \mathbf{e}_i^T \mathbf{Q} \mathbf{e}_i \tag{9}$$

where $\mathbf{Q} = (3D_{iso}\mathbf{E} - \mathbf{D})/2$ and **E** is the identity tensor. In the principal frame of the diffusion tensor, $\tilde{\mathbf{Q}} = \mathbf{AQA}^{-1}$ is diagonal with elements $Q_{xx} = (D_{yy}+D_{zz})/2$, $Q_{yy} = (D_{xx}+D_{zz})/2$ and $Q_{zz} = (D_{xx}+D_{yy})/2$ and **A** is the unitary transformation matrix that diagonalizes **D** and rotates the arbitrary reference frame to the diffusion reference frame (i.e. $\tilde{\mathbf{e}}_i = \mathbf{Ae}_i$). Whereas $(6D_{kk})^{-1}$ is the time constant for rotational diffusion *around* the *k*th principal axis, $(6Q_{kk})^{-1}$ is the average time constant for rotational diffusion *of* the *k*th principal axis. For an asymmetric top, Eq. 9 expands to

$$\begin{aligned} D_i = {} & Q_{11}x_i^2 + Q_{22}y_i^2 + Q_{33}z_i^2 \\ & + 2Q_{12}x_iy_i + 2Q_{13}x_iz_i + 2Q_{23}y_iz_i \end{aligned} \tag{10}$$

As described by Brüschweiler et al. (1995), Eq. 10 is solved by standard linear least-squares optimization for Q_{jk}; the resulting tensor **Q** is diagonalized to determine the eigenvalues Q_{xx}, Q_{yy} and Q_{zz} and the transformation matrix **A**; the diffusion constants, D_{xx}, D_{yy}, and D_{zz}, are determined from the eigenvalues; and θ, ϕ, and ψ are determined from **A**. For a symmetric top, Eq. 9 reduces to

$$D_i = (D_\perp + D_\parallel)/2 + (D_\perp - D_\parallel)(a_{31}x_i + a_{32}y_i + a_{33}z_i)^2/2 \tag{11}$$

where $a_{31} = \sin\theta\cos\phi$, $a_{32} = \sin\theta\sin\phi$, and $a_{33} = \cos\theta$ are elements of **A**. The values of $D_\perp$, $D_\parallel$, θ, and ϕ are determined by nonlinear least-squares optimization. For a spherical top, $\mathbf{D} = D_{iso}\mathbf{E}$ and Eq. 9 reduces to

$$D_i = D_{iso} \tag{12}$$

The least-squares estimator for D_{iso} is the weighted mean of the D_i. As in the direct R_2/R_1 fitting approach, χ^2- and F-statistics are used to evaluate the significance of the isotropic, axial, and anisotropic diffusion models (vide infra).

In the principal axis system of the diffusion tensor, $Q_{12} = Q_{13} = Q_{23} = 0$ and Eq. 10 reduces to

$$\begin{aligned} D_i = {} & Q_{xx}\tilde{x}_i^2 + Q_{yy}\tilde{y}_i^2 + Q_{zz}\tilde{z}_i^2 \\ = {} & D_{iso} - (D_{xx}-D_{yy})\left\{Y_2^2(\tilde{\theta}_i,\tilde{\phi}_i) + Y_2^{-2}(\tilde{\theta}_i,\tilde{\phi}_i)\right\}/(24)^{1/2} \\ & - Y_2^0(\tilde{\theta}_i)(2D_{zz} - D_{xx} - D_{yy})/6 \end{aligned} \tag{13}$$

where $D_{iso} = \mathrm{Trace}\{\mathbf{D}\}/3$, $Y_2^0(\theta) = (3\cos^2\theta - 1)/2$ and $Y_2^{\pm 2}(\theta,\phi) = (3/8)^{1/2}\sin^2\theta\exp(\pm 2i\phi)$ are modified spherical harmonic functions (Brink and Satchler, 1993), and $\{\tilde{\theta}_i, \tilde{\phi}_i\}$ define the orientation of the bond vector in the principal axis

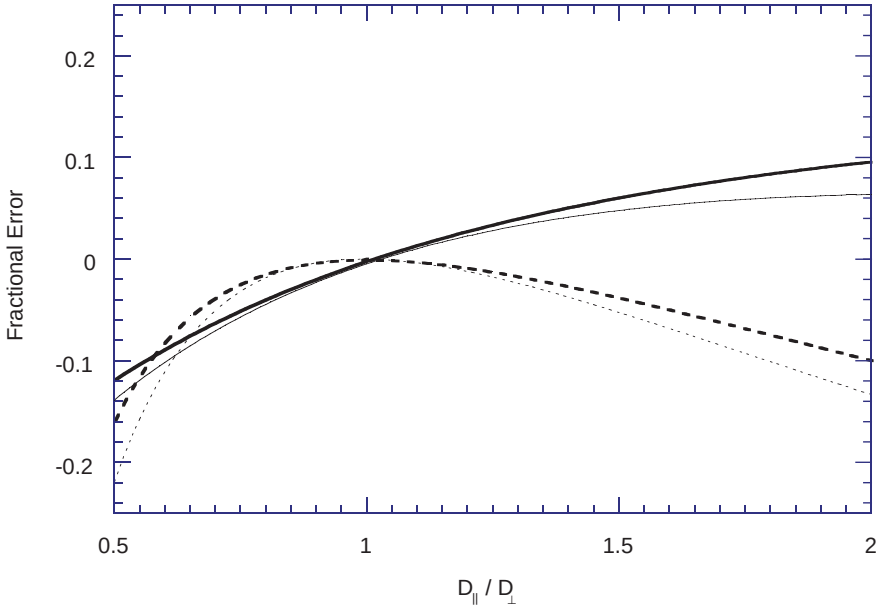

Fig. 1. Fractional errors in D_{iso} (solid lines) and $D_{\parallel}/D_{\perp}$ (dashed lines) determined using the local diffusion approximation are plotted as a function of the actual value of $D_{\parallel}/D_{\perp}$. The results are shown for actual values of D_{iso} equal to 4.2×10^7 s^{-1} (thin lines) and 1.1×10^7 s^{-1} (thick lines).

frame. For axial symmetry, Eq. 13 reduces to

$$D_i = D_{iso} - Y_2^0(\tilde{\theta}_i)\,(D_{\parallel}-D_{\perp})/3 \qquad (14)$$

which provides a straightforward method to evaluate the distribution of bond vector orientations in the diffusion frame after the analysis has been performed. A similar diagnostic relationship can be derived for the direct R_2/R_1 fitting approach in the limit that $\omega_X/(6D_{iso}) \gg 1$:

$$R_{2i}/R_{1i} = (R_{2i}/R_{1i})_{iso}\{1+2Y_2^0(\tilde{\theta}_i)\,(D_{\parallel}/D_{\perp}-1)/3\} \qquad (15)$$

where $(R_{2i}/R_{1i})_{iso}$ is the result for a spherical top with $D_{iso}=(D_{\parallel}+2D_{\perp})/3$.

Direct fitting of the R_2/R_1 ratios is awkward to apply if measurements have been made for different nuclear species or magnetic field strengths because the spectral density functions (Eqs. 4, 7, and 8) appearing in Eq. 3 depend explicitly on the Larmor frequencies, ω_H and ω_X, of the nuclear spins. The local diffusion approach formally separates determination of the D_i from the relaxation rate constants from calculation of the diffusion tensor from the D_i. Thus, data acquired for different nuclear species or at multiple magnetic field strengths can be analyzed simultaneously in a straightforward fashion: the D_i are calculated separately for each set of relaxation rate constants, the $\mathbf{e}_i$ are determined for each bond vector, and the pooled set of $\{D_i,\mathbf{e}_i\}$ is used to calculate the diffusion tensor.

Experimental

Atomic coordinates for human G-CSF (Protein Databank (PDB) entry 1rhg) (Hill et al., 1993) and human ubiquitin (PDB entry 1ubq) (Vijay-Kumar et al., 1987) were obtained from X-ray crystallographic structures. Atomic coordinates for bovine calbindin D_{9k} were obtained from the X-ray crystallographic structure of the major conformer (PDB entry 4icb) (Svensson et al., 1992), from the ensemble of 32 conformations for the $Pro^{43} \rightarrow$ Gly mutant of bovine calbindin D_{9k} derived from NMR spectroscopy (PDB entry 2bcb) (Kördel et al., 1993), and from the energy-minimized average structure of the $Pro^{43} \rightarrow$ Gly mutant of bovine calbindin D_{9k} (PDB entry 2bca) (Kördel et al., 1993). The X-ray crystallographic structure was superposed on the minimized average NMR structure using the C^{α} coordinates for residues in α-helices. The root mean square deviation between the C^{α} positions after superposition was 0.86 Å. Hydrogen atoms were built into the crystal structures using the program INSIGHT II (Molecular Simulations Inc.) by assuming ionization states appropriate for the pH at which the protein crystal structure was obtained (pH 8.7 for calbindin D_{9k}, pH 3.5 for G-CSF, and pH 5.8 for ubiquitin).

^{15}N R_1 and R_2 relaxation rate constants were taken from Tjandra et al. (1995) for human ubiquitin, from Zink et al. (1994) for human G-CSF, and from Kördel et al. (1992) for calbindin D_{9k}.

$^{13}C^{\alpha}$ R_1 and R_2 relaxation rate constants were measured for calbindin D_{9k} using a protein sample that was 15% randomly fractionally enriched with ^{13}C. Isotopically enriched calbindin D_{9k} was produced biosynthetically using 15% randomly ^{13}C enriched glucose as the sole carbon source. Relaxation measurements were performed at a ^1H frequency of 500.13 MHz and a temperature of 300 K using a Bruker AMX500 NMR spectrometer. The pulse sequences utilized have been described elsewhere

(Skelton et al., 1993). The sample was 1.0 mM calbindin D_{9k} in 100% D_2O, pH 5.5 (uncorrected pH meter reading). The R_1 measurements were performed using relaxation delays of 0.010 s (×2), 0.062 s, 0.115 s, 0.194 s, 0.272 s, 0.404 s, 0.535 s, 0.797 s, 1.059 s, 2.109 s (×2), where the notation ×2 indicates that a duplicate data set was acquired for the indicated time point. The R_2 measurements were performed using relaxation delays of 0.004 s (×2), 0.016 s, 0.030 s (×2), 0.050 s, 0.074 s (×2), 0.090 s, 0.108 s, 0.150 s, 0.250 s. Rate constants and uncertainties were obtained by nonlinear least-squares fitting as described elsewhere (Mandel et al., 1995).

Relaxation data for residues exhibiting large-amplitude intramolecular motions were not included in the diffusion tensor calculations. Residues exhibiting significant internal motions on ps–ns time scales were recognized by significant reductions in the $\{^1H\}$-X NOE compared with the average result for the protein; residues exhibiting significant chemical exchange on μs–ms time scales were recognized by significant increases in the values of R_2 compared with the average result for the protein (Tjandra et al., 1995). Residues exhibiting increased internal motions also can be recognized by an examination of the generalized order parameters and phenomenological chemical exchange rate constants after analysis of the relaxation data using the model-free formalism (Lipari and Szabo, 1982a,b; Clore et al., 1990). For calbindin D_{9k}, a total of 60 residues were included in the analysis of the ^{15}N relaxation data; the ^{15}N spins of residues 2–3, 40–45, and 73–75 exhibited increased internal motions, the ^{15}N resonance for residue 1 could not be observed, and the protein contains three proline residues. A total of 47 residues were included in the analysis of the ^{13}C relaxation data; the $^{13}C^{\alpha}$ spins of residues 1–3, 19, 24, 38–44, 47, and 70–75 exhibited increased internal motions and the $^{13}C^{\alpha}$ resonances for residues 7, 8, 18, 28, 33, 49, 57, 59, and 66 could not be quantified due to resonance overlap. The average relative uncertainties in the R_2/R_1 ratios were 1.5% for ^{15}N and 3.3% for $^{13}C^{\alpha}$. For G-CSF, the ^{15}N relaxation rates were included in the analysis only for residues 11–39 in helix A, residues 71–91 in helix B, residues 100–123 in helix C, and residues 143–172 in helix D. Because the published ^{15}N relaxation rates did not include experimental uncertainties (beyond a statement of variation less than 10%), the experimental uncertainties in the R_2/R_1 ratios were set to 0.42 (an average relative uncertainty of 2.5%). The C^{α}-H^{α} bond vectors for all residues in the α-helices were used for model calculations. Analysis of the ^{15}N relaxation rate constants for ubiquitin was performed for the same set of 55 residues used by Tjandra et al. (1995); a relative uncertainty in the R_2/R_1 ratios of 0.78% was derived from the reported average uncertainties in the R_1 and R_2 measurements (Tjandra et al., 1995). The C^{α}-H^{α} bond vectors for all residues in the α-helices and β-sheet were used for model calculations.

Local diffusion constants, $D_i = (6\tau_{ci})^{-1}$, were calculated from the R_{2i}/R_{1i} ratios using Brent's method (Press et al., 1992) to solve Eqs. 3 and 8. The values of D_i derived from ^{13}C relaxation data were scaled empirically by the average ratio of the diffusion constants derived from ^{15}N and ^{13}C relaxation measurements to account for viscosity differences between H_2O and D_2O; the empirical viscosity scaling factor of 17% is slightly smaller than the literature value of 22% (Viswanath and Natarajan, 1989).

Least-squares fits of D_i to Eqs. 10–12 to determine the diffusion tensor for asymmetric, symmetric, and spherical rotators, respectively, were performed as described above using $\mathbf{e}_i$ derived from structural coordinates. Equation 10 was solved for the elements of the anisotropic diffusion tensor by singular value decomposition; uncertainties in parameter estimates were determined by Monte Carlo simulations (Press et al., 1992). Nonlinear least-squares optimization of the axially symmetric diffusion tensor, Eq. 11, was performed using the Levenberg–Marquardt algorithm and uncertainties in parameter estimates were obtained from the covariance matrix (Press et al., 1992) or from jackknife simulations (Mosteller and Tukey, 1977). The weighted mean and the standard error in the mean were used to determine D_{iso} for isotropic diffusion from Eq. 12. For comparison, least-squares fits of the R_{2i}/R_{1i} ratios to Eq. 3 using Eqs. 7 and 8 for axially symmetric and isotropic diffusion tensors, respectively, were

TABLE 1
DIFFUSION PARAMETERS FOR CALBINDIN D_{9k} FROM ^{15}N RELAXATION[a]

Tensor	D_{iso} (10^{-7} s^{-1})	$2D_{zz}/(D_{xx}+D_{yy})$	D_{xx}/D_{yy}	θ (rad)[b]	φ (rad)[b]	ψ (rad)[b]	χ^2	F[c]
Isotropic[d]	3.91 ± 0.01	–	–	–	–	–	179	–
Axial[e]	3.92 ± 0.01	1.08 ± 0.01	–	1.21 ± 0.09	0.18 ± 0.10	–	127	7.62
Anisotropic	3.93 ± 0.01	1.08 ± 0.01	1.04 ± 0.02	1.19 ± 0.36	3.04 ± 0.14	–0.18 ± 0.20	122	0.95

[a] Values of D_i for 60 residues were fit using the local diffusion approximation.
[b] The angles θ, φ, and ψ define the orientation of the diffusion tensor with respect to the coordinate frame of the X-ray crystallographic structure of the major form of calbindin D_{9k}. The structural coordinates obtained from the PDB coordinate file 4icb were superposed on the minimized mean NMR structure (2bca) using the coordinates of the C^{α} spins in α-helical residues.
[c] The F-test indicates that the axially symmetric model is a significant improvement over the isotropic model ($p = 2.3 \times 10^{-4}$). The anisotropic model is not a significant improvement over the axially symmetric model ($p = 0.40$).
[d] $D_{iso} = D_{xx} = D_{yy} = D_{zz}$.
[e] $D_{\parallel} = D_{zz}$, $D_{\perp} = D_{xx} = D_{yy}$, $D_{iso} = (D_{\parallel} + 2D_{\perp})/3$, $D_{\parallel}/D_{\perp} = 2D_{zz}/(D_{xx}+D_{yy})$.

TABLE 2
DIFFUSION PARAMETERS FOR G-CSF FROM ^{15}N RELAXATION[a]

Tensor	D_{iso} (10^{-7} s^{-1})	$2D_{zz}/(D_{xx}+D_{yy})$	D_{xx}/D_{yy}	θ (rad)[b]	φ (rad)[b]	ψ (rad)[b]	χ^2	F[c]
Isotropic[d]	1.28 ± 0.01	–	–	–	–	–	715	–
Axial[d]	1.34 ± 0.01	1.31 ± 0.02	–	1.34 ± 0.03	2.95 ± 0.04	–	504	4.59
Anisotropic	1.35 ± 0.01	1.35 ± 0.03	1.20 ± 0.07	1.76 ± 0.09	–0.31 ± 0.70	0.14 ± 0.10	491	0.39

[a] Values of D_i for 37 residues were fit using the local diffusion approximation.
[b] The angles θ, φ, and ψ define the orientation of the diffusion tensor with respect to the coordinate frame of the X-ray crystallographic structure of G-CSF obtained from the PDB coordinate file 1rhg.
[c] The F-test indicates that the axially symmetric model is a significant improvement over the isotropic model ($p = 8.6 \times 10^{-3}$). The anisotropic model is not a significant improvement over the axially symmetric model ($p = 0.68$).
[d] See Table 1.

performed as described above using the Levenberg–Marquardt algorithm for least-squares optimization (Press et al., 1992). Uncertainties in parameter estimates were obtained from the covariance matrix (Press et al., 1992).

For N spins and m fitted parameters (m = 1, 4, and 6 for isotropic, axially symmetric, and anisotropic diffusion models, respectively), the goodness-of-fit is measured by the χ^2-statistic:

$$\chi^2_{N-m} = \sum_{i=1}^{N} \left(X_i - \hat{X}_i \right)^2 / \sigma_i^2 \qquad (16)$$

where $N - m$ is the number of degrees of freedom, $X_i = D_i$ or R_{2i}/R_{1i} as appropriate, $\hat{X}_i$ is the corresponding fitted value, and σ_i is the uncertainty in X_i. The reduced χ^2-statistic, $\chi^2_r = \chi^2_{N-m}/(N-m)$, has an expectation value of unity. The improvement in the statistical fit to the experimental data afforded by a second diffusion model with $n > m$ parameters is tested using an F-statistic with $n - m$, $N - n$ degrees of freedom:

$$F_{n-m,N-n} = \frac{(\chi^2_{N-m} - \chi^2_{N-n})(N-n)}{\chi^2_{N-n}(n-m)} \qquad (17)$$

Statistical significance of the test statistics is determined by the p-value: the probability that the observed value of the test statistic would be equaled or exceeded by random chance. If $p \leq \alpha$, then the test statistic is significant at the $(1 - \alpha)$% confidence level (Devore, 1982).

In order to evaluate the performance of the local diffusion formalism, selected values of D_{xx}, D_{yy}, and D_{zz} were used to simulate R_{2i}/R_{1i} for randomly oriented N-H bond vectors using Eqs. 3–8. In some instances, arbitrarily chosen rotations were applied to the N-H bond vectors after calculating R_{2i}/R_{1i}. Simulated values of D_i were calculated from the simulated R_{2i}/R_{1i} data, and the diffusion tensor was calculated from the D_i values and bond vector orientations.

Results and Discussion

The approximations inherent in the local diffusion formalism were examined by analyzing simulated data for a symmetric top. As expected (Brüschweiler et al., 1995), the local diffusion method is accurate, provided the degree of rotational anisotropy is not large. As shown in Fig. 1, the estimated value of $D_\parallel/D_\perp$ is always smaller than the actual $D_\parallel/D_\perp$, and the errors in the calculated $D_\parallel/D_\perp$ ratio are less than 10% for $0.65 \ll D_\parallel/D_\perp \ll 1.75$. Errors in the calculated value of D_{iso} are less than 10% over this range of anisotropies as well. The errors in the estimated values of $D_\parallel/D_\perp$ and D_{iso} are only weakly dependent on the actual value of D_{iso}. If desired, the smooth functional relationship between the measured and actual values of $D_\parallel/D_\perp$ and D_{iso} can be used to obtain correction factors for the measured parameters.

The results of the local diffusion analysis of the ^{15}N relaxation data for calbindin D_{9k}, G-CSF, and ubiquitin

TABLE 3
DIFFUSION PARAMETERS FOR UBIQUITIN FROM^{15}N RELAXATION[a]

Tensor	D_{iso} (10^{-7} s^{-1})	$2D_{zz}/(D_{xx}+D_{yy})$	D_{xx}/D_{yy}	θ (rad)[b]	φ (rad)[b]	ψ (rad)[b]	χ^2	F[c]
Isotropic[d]	4.05 ± 0.01	–	–	–	–	–	1051	–
Axial[d]	4.01 ± 0.01	1.15 ± 0.01	–	0.71 ± 0.03	0.81 ± 0.05	–	638	11.00
Anisotropic	4.02 ± 0.01	1.16 ± 0.01	1.04 ± 0.01	0.70 ± 0.17	0.83 ± 0.14	0.02 ± 0.10	609	1.09

[a] Values of D_i for 55 residues were fit using the local diffusion approach.
[b] The angles θ, φ, and ψ define the orientation of the diffusion tensor with respect to the coordinate frame of the X-ray crystallographic structure of ubiquitin obtained from the PDB coordinate file 1ubq.
[c] The F-test indicates that the axially symmetric model is a significant improvement over the isotropic model ($p = 1.1 \times 10^{-5}$). The anisotropic model is not a significant improvement over the axially symmetric model ($p = 0.34$).
[d] See Table 1.

TABLE 4
AXIALLY SYMMETRIC DIFFUSION PARAMETERS FROM ANALYSIS OF ^{15}N R_2/R_1 RATIOS[a]

Protein	Residues[b]	D_{iso} (10^{-7} s^{-1})[c]	$D_\parallel/D_\perp$	θ (rad)[d]	φ (rad)[d]	χ^2	F[e]
Calbindin D_{9k}	60	3.95 ± 0.01	1.08 ± 0.01	1.24 ± 0.09	0.17 ± 0.09	130	7.76
G-CSF	37	1.36 ± 0.01	1.32 ± 0.02	1.34 ± 0.04	3.01 ± 0.04	559	4.46
Ubiquitin	55	4.05 ± 0.01	1.16 ± 0.01	0.68 ± 0.03	0.82 ± 0.05	663	10.02

[a] The diffusion tensor was obtained by direct analysis of the R_2/R_1 ratios.
[b] Number of residues used to determine the diffusion tensor.
[c] $D_{iso} = (D_\parallel + 2D_\perp)/3$.
[d] The angles θ and φ define the orientation of the symmetry axis of the diffusion tensor relative to the coordinates of the X-ray crystallographic structures of calbindin D_{9k} (4icb), G-CSF (1rhg), and ubiquitin (1ubq).
[e] The F-statistic compares the quality of the fit for the axially symmetric tensor with that of the isotropic tensor. The axially symmetric model is a significant improvement over the isotropic model for calbindin D_{9k} ($p = 2.0 \times 10^{-4}$), G-CSF ($p = 9.8 \times 10^{-3}$), and ubiquitin ($p = 2.7 \times 10^{-5}$).

are given in Tables 1, 2, and 3, respectively. In all three cases, the F-statistic indicates that the relaxation is best described using an axially symmetric diffusion tensor. For all three proteins, $D_\parallel/D_\perp < 1.4$ and the local diffusion approximation is expected to be highly accurate. Table 4 lists the results of the direct R_2/R_1 calculations, assuming an axially symmetric diffusion tensor for calbindin D_{9k}, G-CSF, and ubiquitin. The results of the local diffusion and direct R_2/R_1 analyses agree within experimental uncertainties. In all cases, the values of χ^2 are significantly larger than expected statistically, and jackknife simulations (Mosteller and Tukey, 1977) suggest that the reported uncertainties in the results consequently may be underestimated by 30–100% for calbindin D_{9k}, 300–400% for G-CSF, and 300–400% for ubiquitin. Similar increases in parameter uncertainties are obtained by scaling the experimental uncertainties in the D_i to yield $\chi^2_r = 1$ (Press et al., 1992); for example, the uncertainties in D_{iso}, $D_\parallel/D_\perp$, θ, and φ are increased to 0.03, 0.09, 0.14, and 0.15, respectively, for G-CSF. The F-statistic is a ratio of χ^2-statistics and is unaffected by scaling of the experimental uncertainties.

The sensitivity of the diffusion tensor to variations in the orientations of the N-H bond vectors was examined by calculating the axially symmetric diffusion tensor using different structural models of calbindin D_{9k}. Table 5 lists results obtained using atomic coordinates derived from the X-ray crystallographic structure, results obtained using atomic coordinates derived from the minimized average NMR solution structure, and results obtained by averaging calculations performed for each member of the ensemble of 32 NMR solution structures. The diffusion tensors derived using the different sets of coordinates are statistically indistinguishable. Within the ensemble of 32 solution structures, the χ^2 values range from 126 to 155, and the F-statistics range from 4.23 to 9.43. The ranges of χ^2 and F encompass the values obtained using the X-ray crystallographic structure and the minimized average NMR structure. The sample deviations of the elements of the diffusion tensor and rotation angles, calculated from the fitted values for each member of the ensemble, are approximately one-half of the weighted mean uncertainties in the parameters, calculated from the covariance matrix for each member of the ensemble. By extension, approximately one-half of the uncertainty in the measured parameters may be attributable to coordinate uncertainties.

For accurate assessment of the diffusion tensor, the orientations of the bond vectors must be distributed over the surface of a sphere; in particular, as shown by Eqs. 13

TABLE 5
STRUCTURE DEPENDENCE OF AXIALLY SYMMETRIC DIFFUSION PARAMETERS FOR CALBINDIN D_{9k} [a]

Structure	D_{iso} (10^{-7} s^{-1})[b]	$D_\parallel/D_\perp$	θ (rad)[c]	φ (rad)[c]	χ^2	F[d]
NMR average[e]	3.93 ± 0.01	1.07 ± 0.01	1.14 ± 0.10	0.17 ± 0.11	140	5.18
NMR ensemble[f]	3.92 ± 0.01 (0.004)	1.08 ± 0.01 (0.006)	1.27 ± 0.09 (0.05)	0.16 ± 0.10 (0.04)	133	6.38
X-ray[g]	3.92 ± 0.01	1.08 ± 0.01	1.21 ± 0.09	0.18 ± 0.10	127	7.62

[a] Values of D_i for 60 residues were fit using the local diffusion approach.
[b] $D_{iso} = (D_\parallel + 2D_\perp)/3$.
[c] The angles θ and φ define the orientation of the symmetry axis of the diffusion tensor.
[d] The F-statistic compares the quality of the fit for the axially symmetric tensor with that of the isotropic tensor. The axially symmetric model is a significant improvement over the isotropic model in all three instances.
[e] The NMR average structure of the $Pro^{43} \rightarrow Gly$ mutant was obtained from the coordinate file 2bca.
[f] The ensemble of 32 NMR solution structures of the $Pro^{43} \rightarrow Gly$ mutant was obtained from the coordinate file 2bcb. The weighted mean values and uncertainties from 32 individual fits are shown. The values in parentheses are the sample deviations calculated over the ensemble.
[g] The X-ray crystallographic structure of wild-type calbindin D_{9k} was obtained from coordinate file 4icb. The coordinates for the major conformer were utilized. The structural coordinates were superposed on the minimized mean NMR structure (2bca) using the coordinates of the C^α spins in α-helical residues.

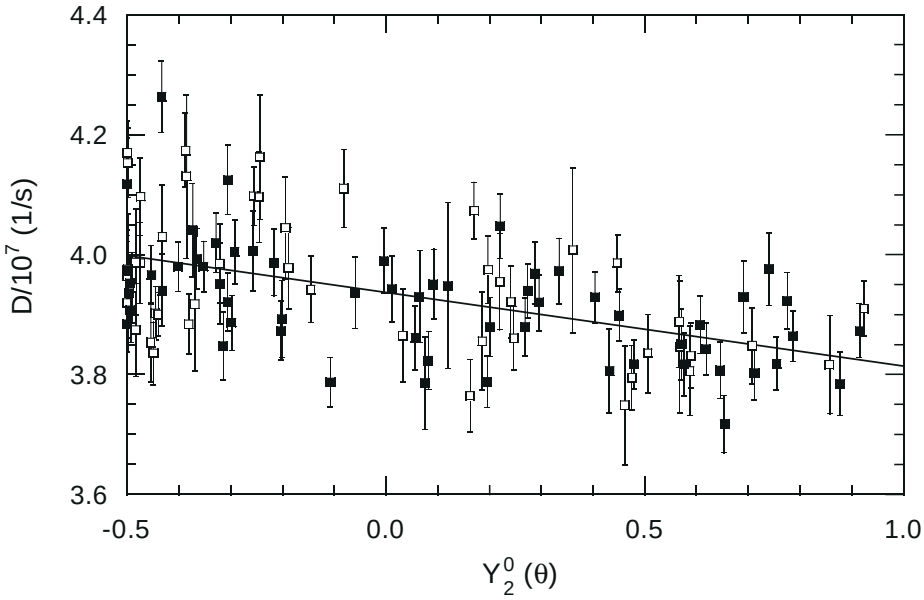

Fig. 2. Axially symmetric diffusion for calbindin D_{9k}. The values of D_i obtained from ^{15}N (■) and ^{13}C (□) relaxation experiments are shown as functions of $Y_2^0(\theta)$. The values of θ_i were obtained after rotating the structural coordinates to the principal axis frame of the diffusion tensor using the transformation matrix obtained from the local diffusion analysis. The solid line is the simultaneous least-squares fit of Eq. 14 to the experimental data.

and 14, the bond vector orientations should sample the full range of the spherical harmonic functions. Figures 2, 3, and 4 plot D_i derived from the ^{15}N relaxation data versus $Y_2^0(\tilde{\theta}_i)$ for the N-H bond vectors. These results indicate the three possible orientational distributions encountered in proteins. For calbindin D_{9k}, N-H bond vector orientations are distributed reasonably well over the full range $-0.5 \le Y_2^0(\tilde{\theta}_i) \le 1.0$. In contrast, for G-CSF, the N-H bond vectors are preferentially oriented along the axes of the helices. Consequently, the majority of bond vectors have $0 \le Y_2^0(\tilde{\theta}_i) \le 1.0$, corresponding to an angular range $0.955\ \text{rad} \ge \theta \ge 0\ \text{rad}$ or $\pi - 0.955\ \text{rad} \le \theta \le \pi$.

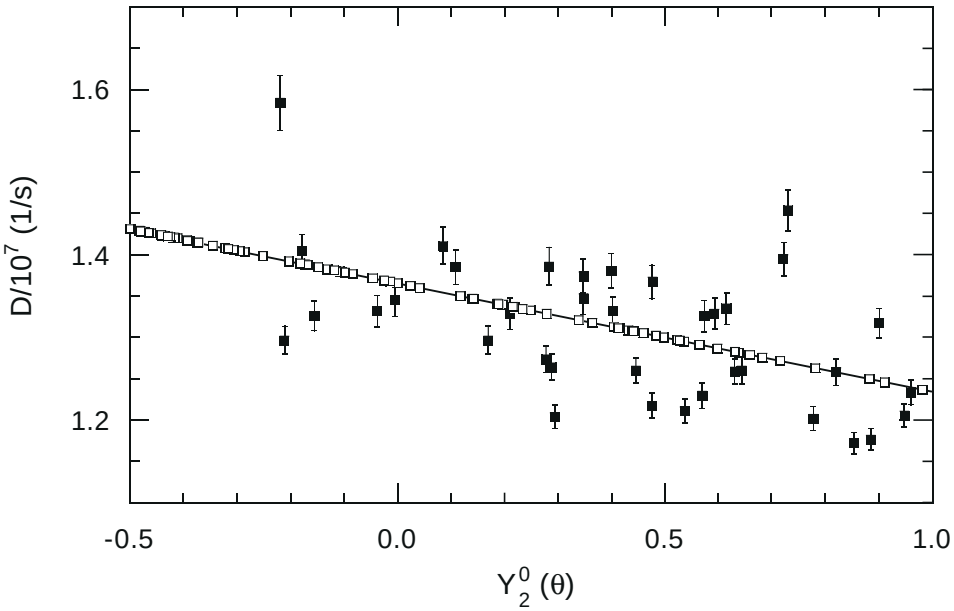

Fig. 3. Axially symmetric diffusion for G-CSF. The D_i values obtained from ^{15}N (■) relaxation experiments are shown as functions of $Y_2^0(\theta)$. The values of θ_i were obtained after rotating the structural coordinates to the principal axis frame of the diffusion tensor using the transformation matrix obtained from the local diffusion analysis. The solid line is the least-squares fit of Eq. 14 to the experimental data. The predominance of values of $Y_2^0(\theta) > 0$ stems from the four-helix bundle topology of G-CSF. The theoretical values of D_i obtainable from ^{13}C (□) relaxation measurements are shown as functions of $Y_2^0(\theta)$ for residues located within secondary structure.

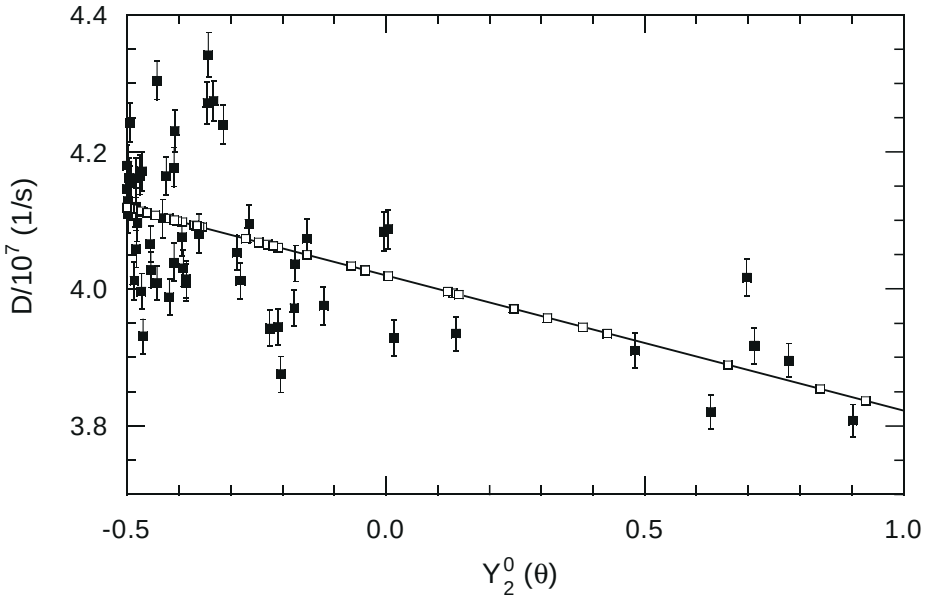

Fig. 4. Axially symmetric diffusion for ubiquitin. The D_i values obtained from ^{15}N (■) relaxation experiments are shown as functions of $Y_2^0(\theta)$. The values of θ_i were obtained after rotating the structural coordinates to the principal axis frame of the diffusion tensor using the transformation matrix obtained from the local diffusion analysis. The solid line is the least-squares fit of Eq. 14 to the experimental data. The predominance of values of $Y_2^0(\theta) < 0$ stems from the orientation of the α-helices and β-sheets with respect to the unique diffusion axis. The theoretical values of D_i obtainable from ^{13}C (□) relaxation measurements are shown as functions of $Y_2^0(\theta)$ for residues located within secondary structure.

For ubiquitin, the majority of N-H bond vectors have $-0.5 \leq Y_2^0(\theta) \leq 0$, corresponding to an angular range $0.955 \text{ rad} \leq \theta \leq \pi - 0.955 \text{ rad}$, and are nearly perpendicular to the unique axis of the diffusion tensor. The importance of the distribution of orientations of the bond vectors is illustrated by the following simple calculations. For G-CSF, if the six N-H bond vectors with $Y_2^0(\tilde{\theta}_i) \leq 0$ are excluded from the analysis, the uncertainties in the measured parameters for the axially symmetric diffusion tensor increase, and the F-statistic comparing the axially symmetric and isotropic models is reduced from 4.59 ($p = 8.6 \times 10^{-3}$) to 2.21 ($p = 0.11$). In this case, the axially symmetric and isotropic models can no longer be distinguished statistically. For ubiquitin, if the eight N-H vectors with $Y_2^0(\tilde{\theta}_i) \geq 0$ are excluded from the analysis, the uncertainties in the measured parameters for the axially symmetric diffusion tensor increase, and the F-statistic comparing the axially symmetric and isotropic models is reduced from 11.00 ($p = 1.1 \times 10^{-5}$) to 3.79 ($p = 0.017$).

The distribution of bond vector orientations is improved by the inclusion of data for C^α-H^α bond vectors together with data for N-H bond vectors. This advantage was demonstrated empirically for calbindin D_{9k}, by performing the local diffusion analysis with separate ^{13}C and ^{15}N data sets and with a combined $^{13}C/^{15}N$ data set. The results are shown in Tables 1, 6, and 7 for ^{13}C, ^{15}N, and $^{13}C/^{15}N$ data sets, respectively, using coordinates derived from the X-ray crystallographic structure of calbindin D_{9k}. The values of the $^{13}C^\alpha$ relaxation rate constants used in the analysis are given in Table 8. A comparison of the

TABLE 6
DIFFUSION PARAMETERS FOR CALBINDIN D_{9k} FROM ^{13}C RELAXATION[a]

Tensor	D_{iso} (10^{-7} s^{-1})	$2D_{zz}/(D_{xx}+D_{yy})$	D_{xx}/D_{yy}	θ (rad)[b]	φ (rad)[b]	ψ (rad)[b]	χ^2	F[c]
Isotropic[d]	3.36 ± 0.01	–	–	–	–	–	143	
Axial[d]	3.35 ± 0.01	1.10 ± 0.02	–	1.40 ± 0.10	–0.20 ± 0.10	–	112	3.84
Anisotropic	3.35 ± 0.01	1.10 ± 0.02	1.01 ± 0.01	1.75 ± 0.20	0.21 ± 0.22	–0.27 ± 0.24	112	0.0

[a] Values of D_i for 47 residues were fit using the local diffusion approximation. Results are not scaled for differences in viscosity between D_2O and H_2O; D_{iso} should be multiplied by 1.17 for comparison with results in H_2O.

[b] The angles θ, φ, and ψ define the orientation of the diffusion tensor with respect to the coordinate frame of the X-ray crystallographic structure of the major form of calbindin D_{9k}. The structural coordinates obtained from the PDB coordinate file 4icb were superposed on the minimized mean NMR structure (2bca) using the coordinates of the C^α spins in α-helical residues.

[c] The F-test indicates that the axially symmetric model is a significant improvement over the isotropic model ($p = 0.016$). The anisotropic model is not a significant improvement over the axially symmetric model.

[d] See Table 1.

TABLE 7
DIFFUSION PARAMETERS FOR CALBINDIN D_{9k} FROM COMBINED ^{13}C AND ^{15}N RELAXATION[a]

Tensor	D_{iso} (10^{-7} s^{-1})	$2D_{zz}/(D_{xx}+D_{yy})$	D_{xx}/D_{yy}	θ (rad)[b]	φ (rad)[b]	ψ (rad)[b]	χ^2	F[c]
Isotropic[d]	3.92 ± 0.01	–	–	–	–	–	333	–
Axial[d]	3.93 ± 0.01	1.08 ± 0.01	–	1.25 ± 0.06	0.04 ± 0.07	–	251	11.2
Anisotropic	3.93 ± 0.01	1.08 ± 0.01	1.03 ± 0.01	1.25 ± 0.31	−3.14 ± 0.08	−0.08 ± 0.14	247	0.92

[a] Values of D_i for 108 bond vectors were fit using the local diffusion approximation. Values of D_i for $^{13}C^{\alpha}$-H^{α} bond vectors were multiplied by 1.17 prior to analysis to account for the viscosity difference between H_2O and D_2O.
[b] See Table 6.
[c] The F-test indicates that the axially symmetric model is a significant improvement over the isotropic model ($p = 2.1 \times 10^{-6}$). The anisotropic model is not a significant improvement over the axially symmetric model ($p = 0.40$).
[d] See Table 1.

results in Tables 1, 6, and 7 shows the improvement afforded by the simultaneous analysis of ^{13}C and ^{15}N data. The distribution of C^{α}-H^{α} bond vectors is illustrated in Fig. 2. The statistical significance of the axially symmetric diffusion model, compared with the isotropic model, is improved in the simultaneous analysis: the p-value for the F-statistic is reduced from 5.0×10^{-3} for the ^{15}N analysis to 1.7×10^{-5} for the combined $^{13}C/^{15}N$ analysis. Because the N-H bond vectors are distributed reasonably uniformly in calbindin D_{9k}, much of the improvement in the precision of the results arises from the increased number of bond vectors available for analysis. To further demonstrate the advantage of combining ^{13}C data with ^{15}N data for proteins with less ideal distributions of N-H bond vectors, the diffusion tensor and transformation matrix determined from ^{15}N relaxation measurements for G-CSF and ubiquitin were used to calculate theoretical values of D_i and θ_i for the C^{α}-H^{α} bond vectors for residues within stable secondary structures, as noted above. The results are overlaid on the distributions of D_i and θ_i for the N-H bond vectors in Figs. 3 and 4. The improved distribution of bond vector orientations is most striking for G-CSF because the angle between the two bond vectors (not the dihedral angle) is 0.98 rad (56°) for an α-helix (the corresponding angle is 2.72 rad (156°) for a β-sheet).

A close inspection of the results in Tables 1, 6, and 7 for ^{15}N, $^{13}C^{\alpha}$, and combined ^{15}N and $^{13}C^{\alpha}$ analyses indicates that the $D_{\parallel}/D_{\perp}$ ratios are in better agreement than θ or φ (the D_{iso} values are related by the empirical scaling for viscosity differences). For example, the angle between the symmetry axes of the diffusion tensors determined from separate analyses of ^{15}N and $^{13}C^{\alpha}$ relaxation data is 0.40 rad (23°), as determined from the scalar product of unit vectors along the symmetry axes. Similar calculations (not shown) yield 0.43 rad (25°) and 0.29 rad (17°) for separate analyses of ^{15}N and $^{13}C^{\alpha}$ relaxation data using the minimized mean NMR solution structure and the ensemble of 32 NMR solution structures, respectively. The orientations of the symmetry axes of the diffusion tensors are illustrated in Fig. 5. As noted above, the large χ^2 values obtained in all analyses suggest that the uncertainties in the fitted parameters are underestimated; consequently, the variation in orientation of the symmetry axes of diffusion tensors calculated separately for ^{15}N and $^{13}C^{\alpha}$ may provide a more realistic estimate of the precision of the methods. The difference in orientations also is a consequence of the shallow χ^2 response surface for calbindin D_{9k} that results from the small degree of anisotropy of the molecule and the larger uncertainties in the $^{13}C^{\alpha}$ relaxation data (1.9% average relative uncertainty in τ_{ci} for $^{13}C^{\alpha}$ data compared to 1.4% for ^{15}N data). If the

TABLE 8
CALBINDIN D_{9k} ^{13}C RELAXATION PARAMETERS

Residue	R_1 (s^{-1})	R_2 (s^{-1})	Residue	R_1 (s^{-1})	R_2 (s^{-1})
K1	2.44 ± 0.06	20.6 ± 0.5	S38	2.12 ± 0.05	16.5 ± 0.5
S2	2.26 ± 0.04	17.9 ± 0.2	L39	2.23 ± 0.04	19.9 ± 0.3
P3	2.07 ± 0.02	19.3 ± 0.3	L40	2.33 ± 0.03	17.4 ± 0.4
E4	2.11 ± 0.03	20.5 ± 0.3	K41	2.41 ± 0.02	14.7 ± 0.3
E5	2.21 ± 0.04	20.6 ± 0.3	S44	2.43 ± 0.02	16.1 ± 0.4
L6	2.16 ± 0.04	20.1 ± 0.4	T45	2.21 ± 0.06	22.4 ± 0.3
I9	2.04 ± 0.05	20.6 ± 0.3	L46	2.07 ± 0.07	22.6 ± 0.5
F10	1.95 ± 0.04	20.9 ± 0.6	D47	2.10 ± 0.05	24.0 ± 0.5
E11	2.02 ± 0.04	21.6 ± 0.4	E48	2.07 ± 0.07	21.2 ± 0.3
K12	1.96 ± 0.05	20.4 ± 0.2	F50	1.95 ± 0.04	21.1 ± 0.5
Y13	2.08 ± 0.03	22.0 ± 0.4	E51	2.15 ± 0.04	20.1 ± 0.8
A14	1.94 ± 0.03	21.4 ± 0.4	E52	2.00 ± 0.04	20.6 ± 0.3
A15	1.87 ± 0.06	18.4 ± 0.3	L53	2.04 ± 0.05	23.0 ± 1.0
K16	2.08 ± 0.03	20.0 ± 0.3	D54	1.94 ± 0.05	20.7 ± 0.5
E17	2.06 ± 0.06	20.4 ± 0.5	K55	1.98 ± 0.05	20.0 ± 0.3
D19	1.97 ± 0.03	23.5 ± 0.5	N56	2.02 ± 0.02	21.2 ± 0.3
P20	1.95 ± 0.03	21.1 ± 0.4	D58	1.99 ± 0.05	21.4 ± 0.3
N21	1.91 ± 0.04	20.7 ± 0.3	E60	2.13 ± 0.03	20.0 ± 0.4
Q22	2.01 ± 0.06	20.1 ± 1.0	V61	2.11 ± 0.04	20.0 ± 1.1
L23	2.16 ± 0.05	21.8 ± 0.7	S62	2.09 ± 0.06	22.2 ± 0.5
S24	2.07 ± 0.04	24.3 ± 0.7	F63	2.05 ± 0.04	20.9 ± 0.5
K25	2.02 ± 0.03	20.5 ± 0.4	E64	2.00 ± 0.03	20.9 ± 0.3
E26	2.04 ± 0.03	21.4 ± 0.3	E65	2.09 ± 0.04	21.5 ± 0.4
E27	1.94 ± 0.07	20.2 ± 0.8	Q67	2.04 ± 0.03	20.6 ± 0.3
K29	2.06 ± 0.04	22.1 ± 0.5	V68	2.05 ± 0.05	19.6 ± 0.3
L30	2.09 ± 0.04	20.1 ± 0.4	L69	2.12 ± 0.05	20.4 ± 0.5
L31	2.02 ± 0.04	22.6 ± 0.5	V70	2.13 ± 0.05	17.8 ± 0.3
L32	1.96 ± 0.07	21.1 ± 0.7	K71	2.11 ± 0.07	18.8 ± 0.5
T34	2.05 ± 0.03	20.8 ± 0.8	K72	2.56 ± 0.09	16.2 ± 0.3
E35	2.01 ± 0.04	20.9 ± 0.4	I73	2.43 ± 0.02	15.6 ± 0.2
F36	1.98 ± 0.05	20.9 ± 0.5	S74	2.61 ± 0.04	12.1 ± 0.1
P37	1.86 ± 0.03	20.4 ± 0.6			

$^{13}C^{\alpha}$ data are analyzed by fixing the values of θ and ϕ at the values obtained from the ^{15}N analysis, then the χ^2-statistic increases to 124, an increase of only 12, and the degree of improvement compared to the isotropic model is essentially unchanged ($F = 6.91$, $p = 0.012$) because the number of fitted parameters is reduced by two.

The ^{15}N NMR spectrum is usually better resolved than the ^{13}C NMR spectrum of proteins; consequently, as observed for calbindin D_{9k}, relaxation data suitable for the diffusion tensor analysis may be available for a larger number of ^{15}N resonances than $^{13}C^{\alpha}$ resonances. In the worst case, the distribution of orientations of the $^{13}C^{\alpha}$-H^{α} bond vectors for resolved, quantifiable, $^{13}C^{\alpha}$ spins might not improve upon the distribution of ^{15}N spins, in which case the simultaneous analysis would be expected to improve the precision, but not the accuracy, of the diffusion tensor. Normally, structural coordinates are available from X-ray or NMR experiments and the ^{15}N and ^{13}C NMR spectra are assigned prior to collecting relaxation data; therefore, the number of resolved resonances and the distribution of the corresponding bond vectors can be ascertained in advance.

Analysis of simulated relaxation data indicates that anisotropic rotational diffusion can be detected with D_{xx}/D_{yy} as small as 1.05 if the distribution of bond vectors is uniform and if the uncertainties in the R_2/R_1 ratios are ~1%. For example, 10 sets of R_2/R_1 relaxation data for 50 randomly oriented bond vectors were simulated and analyzed using $D_{iso} = 4.0 \times 10^7$ s^{-1}, $2D_{zz}/(D_{xx} + D_{yy}) = 1.10$, $D_{xx}/D_{yy} = 1.05$, and a random noise level of 1%. The average F-statistic for the axially symmetric diffusion model compared with the isotropic model was 33.6 ($p = 1.2 \times 10^{-11}$), and the F-statistic for the anisotropic diffusion model compared with the axially symmetric diffusion model was 5.83 ($p = 5.7 \times 10^{-3}$). In contrast, axially symmetric diffusion tensors provided statistically sufficient descriptions of the overall rotational diffusion for each of the three proteins studied. The proteins have fairly axially symmetric structures as defined by the ratios of the principal components of the inertia tensors for calbindin D_{9k} (1.00:0.874:0.814), G-CSF (1.00:0.976:0.397), and ubiquitin (1.00:0.904:0.636), and the results for the diffusion tensors might not be unexpected. However, *Escherichia coli* ribonuclease H has an asymmetric structure as defined by the ratios of the principal components of the inertia tensor (1.00:0.781:0.631), but analysis of ^{15}N spin relaxation data yields an axially symmetric diffusion tensor nonetheless (Mandel et al., 1996). The failure to observe statistically significant anisotropic diffusion tensors stems from two causes. (i) As illustrated by the above example, statistical improvement of the anisotropic diffusion model compared to the axially symmetric model frequently is smaller, and harder to detect statistically, than the improvement of the axially symmetric model compared to the isotropic model. (ii) The χ^2 values for the experimental data given in Tables 1–7 are larger than expected statistically, which suggests that the measured uncertainties in the relaxation data underestimate the true uncertainties. As a result, the experimental D_i values deviate significantly from the expected linear relationship in Figs. 2–4. An increased variation in the relaxation data reduces the values of the F-statistics for both axially symmetric and anisotropic diffusion models and renders detecting a fully anisotropic diffusion tensor more difficult. For example, if the uncertainty in the R_2/R_1 ratios is increased to 2% in the above simulation, then the F-statistics for axially symmetric and anisotropic diffusion models are reduced to 7.7 ($p = 2.8 \times 10^{-4}$) and 1.9 ($p = 0.16$), respectively. Additional sources of uncertainty in the analysis can arise from variations in CSA values and bond lengths for different N-H vectors in the molecule, coordinate errors, and intramolecular dynamic processes that contribute to R_1 and R_2 and affect Eq. 3. The robust detection of the fully anisotropic rotational diffusion of proteins by the methods outlined herein will require a better understanding of the sources of variation in the relaxation rate constants.

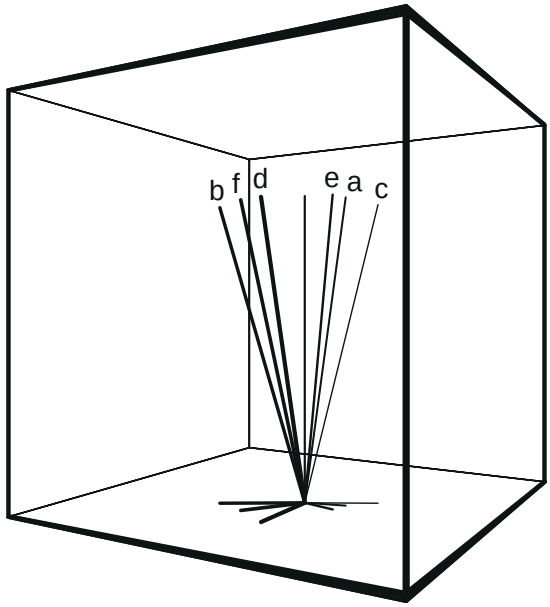

Fig. 5. Symmetry axis orientations for calbindin D_{9k}. Unit vectors along the symmetry axes of the axially symmetric rotational diffusion tensors of calbindin D_{9k} are shown for analyses performed using (a) X-ray structure and ^{15}N relaxation data, (b) X-ray structure and $^{13}C^{\alpha}$ relaxation data, (c) minimized average NMR solution structure and ^{15}N relaxation data, (d) minimized average NMR solution structure and $^{13}C^{\alpha}$ relaxation data, (e) ensemble of 32 NMR solution structures and ^{15}N relaxation data, and (f) ensemble of 32 NMR solution structures and $^{13}C^{\alpha}$ relaxation data. The (unlabeled) z-axis is taken as the direction of the symmetry axis of the diffusion tensor calculated using the X-ray structure and combined ^{15}N and $^{13}C^{\alpha}$ relaxation data. The projections of the unit vectors onto the transverse plane are drawn to illustrate the orientations of the vectors. The angles between the unit vectors and the z-axis are (a) 0.14 rad, (b) 0.28 rad, (c) 0.24 rad, (d) 0.26 rad, (e) 0.12 rad, and (f) 0.22 rad.

Conclusions

A detailed knowledge of the hydrodynamic rotational anisotropy of proteins is important for interpreting relaxation rate constants and constructing structural models of anisotropic molecules (Barbato et al., 1992; Brüschweiler et al., 1995). Rotational anisotropy can affect model selection during the analysis of relaxation data using model-free formalisms, can introduce spurious parameters, and can bias optimized internal motional parameters (Schurr et al., 1994; Mandel et al., 1996). The simultaneous analysis of ^{13}C and ^{15}N relaxation data reduces the bias in the distribution of bond vector orientations used to determine the diffusion tensor. The local diffusion approach for determining the diffusion tensor (Brüschweiler et al., 1995) is emphasized herein because this method is particularly well suited to the analysis of relaxation data acquired for different nuclear species or for different magnetic field strengths. The theoretical and experimental methods described are expected to be widely applicable to hydrodynamic studies of proteins and protein complexes.

Acknowledgements

We thank Eva Thulin for preparing the fractionally ^{13}C enriched sample of calbindin D_{9k}, Mikael Akke (Columbia University) and Ishwar Radhakrishnan (The Scripps Research Institute) for helpful discussions, and Rafael Brüschweiler, Ishwar Radhakrishnan and Peter E. Wright (The Scripps Research Institute) for access to their software Quadric. L.K.L. was supported by the National Institutes of Health M.S.T.P. Grant 5T32-GM-07367. This work was supported by grants from the NSF (MCB 9419049) and from the Arnold and Mabel Beckman Foundation, awarded to A.G.P.; a grant from the NSF (MCB 9221280) awarded to M.R.; and grants from the NIH (GM 40120) and American Cancer Society (FRA-436) awarded to W.J.C. Data analysis software is available from http://convex.hhmi.columbia.edu/palmer_group.html.

References

Abragam, A. (1961) *Principles of Nuclear Magnetism*, Clarendon Press, Oxford, U.K.

Barbato, G., Ikura, M., Kay, L.E., Pastor, R.W. and Bax, A. (1992) *Biochemistry*, **31**, 5269–5278.

Brink, D.M. and Satchler, G.R. (1993) *Angular Momentum*, Clarendon Press, Oxford, U.K.

Brüschweiler, R., Liao, X. and Wright, P.E. (1995) *Science*, **268**, 886–889.

Clore, G.M., Driscoll, P.C., Wingfield, P.T. and Gronenborn, A.M. (1990) *Biochemistry*, **29**, 7387–7401.

Devore, J. (1982) *Probability and Statistics for Engineering and the Sciences*, Brooks/Cole, Monterey, CA, U.S.A.

Farrow, N.A., Muhandiram, R., Singer, A.U., Pascal, S.M., Kay, C.M., Gish, G., Shoelson, S.E., Pawson, T., Forman-Kay, J.D. and Kay, L.E. (1994) *Biochemistry*, **33**, 5984–6003.

Farrow, N.A., Zhang, O., Szabo, A., Torchia, D.A. and Kay, L.E. (1995) *J. Biomol. NMR*, **6**, 153–162.

Hill, C.P., Osslund, T.D. and Eisenberg, D. (1993) *Proc. Natl. Acad. Sci. USA*, **90**, 5167–5171.

Ishima, R. and Nagayama, K. (1995) *J. Magn. Reson.*, **B108**, 73–76.

Kay, L.E., Torchia, D.A. and Bax, A. (1989) *Biochemistry*, **28**, 8972–8979.

Kördel, J., Skelton, N.J., Akke, M., Palmer, A.G. and Chazin, W.J. (1992) *Biochemistry*, **31**, 4856–4866.

Kördel, J., Skelton, N.J., Akke, M. and Chazin, W.J. (1993) *J. Mol. Biol.*, **231**, 711–734.

Lipari, G. and Szabo, A. (1982a) *J. Am. Chem. Soc.*, **104**, 4546–4559.

Lipari, G. and Szabo, A. (1982b) *J. Am. Chem. Soc.*, **104**, 4559–4570.

Mackay, J.P., Shaw, G.L. and King, G.F. (1996) *Biochemistry*, **35**, 4867–4877.

Mandel, A.M., Akke, M. and Palmer, A.G. (1995) *J. Mol. Biol.*, **246**, 144–163.

Mandel, A.M., Akke, M. and Palmer, A.G. (1996) *Biochemistry*, **35**, 16009–16023.

Mosteller, F. and Tukey, J.W. (1977) *Data Analysis and Regression. A Second Course in Statistics*, Addison-Wesley, Reading, MA, U.S.A.

Palmer, A.G., Williams, J. and McDermott, A. (1996) *J. Phys. Chem.*, **100**, 13293–13310.

Peng, J.W. and Wagner, G. (1992) *J. Magn. Reson.*, **98**, 308–332.

Press, W.H., Flannery, B.P., Teukolsky, S.A. and Vetterling, W.T. (1992) *Numerical Recipes. The Art of Scientific Computing*, Cambridge University Press, Cambridge, U.K.

Schurr, J.M., Babcock, H.P. and Fujimoto, B.S. (1994) *J. Magn. Reson.*, **B105**, 211–224.

Skelton, N.J., Palmer, A.G., Akke, M., Kördel, J., Rance, M. and Chazin, W.J. (1993) *J. Magn. Reson.*, **B102**, 253–264.

Svensson, L.A., Thulin, E. and Forsén, S. (1992) *J. Mol. Biol.*, **223**, 601–606.

Tjandra, N., Feller, S.E., Pastor, R.W. and Bax, A. (1995) *J. Am. Chem. Soc.*, **117**, 12562–12566.

Vijay-Kumar, S., Bugg, C.E. and Cook, W.J. (1987) *J. Mol. Biol.*, **194**, 531–544.

Viswanath, D.S. and Natarajan, G. (1989) *Data Book on the Viscosity of Liquids*, Hemisphere, New York, NY, U.S.A.

Woessner, D.E. (1962) *J. Chem. Phys.*, **37**, 647–654.

Zheng, Z., Czaplicki, J. and Jardetzky, O. (1995) *Biochemistry*, **34**, 5212–5223.

Zink, T., Ross, A., Lüers, K., Cieslar, C., Rudolph, R. and Holak, T.A. (1994) *Biochemistry*, **33**, 8453–8463.